AIAA SCITECH 2025 Forum, 6-10 January 2025 Orlando, FL. Paper number AIAA 2025-1842
DOI:10.2514/6.2025-1842

CFD Modelling and Simulation on a Lambda Wing at Subsonic Speed

Simon A. Prince[1], Zeeshan Rana[2], Davide Di Pasquale[3], Claude Podwojewski[4] and Tomas Zielinski[4]
Centre for Aeronautics, School of Aerospace, Transport & Manufacturing, Cranfield University, Bedfordshire, UK.

This paper presents and discusses the results of a study at subsonic airspeed of the aerodynamic characteristics of the Swept Wing Flow Test (SWIFT) lambda wing configuration, which was undertaken as part of the NATO AVT-298 Task Group activity on "Reynolds Number Scaling Effects on Swept Wing Flows". While the task group studied the aerodynamics of this unconventional wing shape across the subsonic and transonic Mach number, and a wide range of Reynolds numbers via cryogenic testing in the NASA NTF wind tunnel, this paper focuses only on the Mach 0.2 conditions at a Reynolds number, based on mean chord, of 2.5 million, for which the model was tested at the ARA Transonic Wind Tunnel in the UK. Various fidelity CFD methods were employed for comparison with experimental data, over a pitch sweep from -4 to 20 degrees angle of attack, including the Viscous Full Potential (VFP) method, RANS, Unsteady RANS and Delayed Detached Eddy Simulation (DDES). The results for this case, highlight the complex 3D stall, initiating inboard, associated with this class of swept wing, which is very different from that seen on conventional swept, tapered wings typically seen on civil transport aircraft, which tends to initiate towards the tip. While the results show that, of the RANS turbulence models tested, the k-ω SST turbulence model most effectively predicted the experimental data, but none of the linear eddy viscosity models could resolve the benign stall characteristics captured in the experiment. Only the DDES method was found to effectively predict the post stall characteristics to some degree of accuracy. The VFP method generated results in a fraction of the time (seconds compared with hours), required for higher fidelity CFD solution, and was found to provide data with equivalent accuracy to RANS based methods for pre-stall conditions.

I. Nomenclature

α	=	angle of attack (deg)
C_p	=	pressure coefficient
C_L	=	Lift coefficient based on planform area.
C_D	=	Drag coefficient based on planform area.
C_M	=	Pitching moment coefficient based on planform area, and reference length of 603 mm
c	=	chord (mm)
$\bar{c}$	=	mean chord (559.1 mm)
dt	=	time step (seconds)
$y+$	=	dimensionless first cell height above wall
x_m	=	x distance to the balance moment center (m)
CFL	=	Courant-Friedrich-Lewy number
$Re_{\bar{c}}$	=	Reynolds number based on mean chord

[1] Professor of Aerodynamics, Senior Member AIAA.
[2] Senior Lecturer, Member AIAA.
[3] Lecturer.
[4] Masters student.

S-A = Spalart-Allmaras turbulence model with QCR correction.
k-ε = k-epsilon turbulence model
k-ω = k-omega turbulence model
SST = shear stress transport
RANS = Reynolds averaged Navier-Stokes
URANS = Unsteady Reynolds averaged Navier-Stokes
DDES = Delayed Detached Eddy Simulation

II. Introduction

Much interest has been focused on the concept of the Blended-Wing-Body aircraft as a configuration that promises a step change in aerodynamic efficiency over and above that of the conventional fuselage / swept and tapered wing configuration. Of the planform designs developed, the lambda wing has been particularly popular. Driven more by the requirements of radar signature than aerodynamic efficiency, early blended wing aircraft configurations employed lambda wing planforms including the B-2 and the F-117 developed in the 1970's and 80's. In addition to stability issues, it was found that these aircraft presented difficult aerodynamic characteristics requiring large control surfaces and having complex 3D stall characteristics very different from those, well understood, seen with swept/tapered high speed wings.

When high resolution computational fluid dynamics (CFD) methods based on the solution of the Navier-Stokes equations became practical, it was found that in many computational studies of these type of configurations Reynolds Averaged Navier-Stokes calculations were found to be unable to properly resolve the complex 3D flows measured in experimental test cases at the higher angles of attack. This was puzzling as these methods were known to be sufficiently rigorous to provide good predictions for swept/tapered wing flows at these conditions – resolving incipient tip separations and subsequent stall evolution, although it was known that higher fidelity was required for unsteady highly separated flow cases. In addition, Reynolds number sensitivity was found to be a significant issue in the 3D flow on these wings, where boundary layer transition and pitch hysteresis were known to be important.

In 2017/18 a NATO AVT activity was launched (AVT-298) to undertake an international collaborative effort to advance our knowledge and available data on the flow around lambda wings. The aim was to derive high quality experimental data across a range of Reynolds numbers and Mach numbers (low speed to transonic), employing the cryogenic NASA National Transonic Facility (NTF) and the Aircraft Research Association (ARA) Transonic Wind Tunnel to investigate these effects, alongside the deployment of some of the worlds most advanced time accurate CFD modelling and simulation codes in an effort to predict the test cases.

Publications are due to present the results of the whole study, comparing all of the experimental data and the computational simulation efforts of the consortia. This paper presents just a selection of results from the contribution to that effort of Cranfield University in the UK. In particular this paper focuses only on the results of a comparative CFD study at low-speed Mach 0.2 condition where the Reynolds number, based on mean chord, was 2.5 million. Here the dominant flow physics of interest was the smooth surface boundary layer separation and subsequent stall development, known to be highly 3D in nature, complex and difficult to predict. The CFD predictions in this paper are compared only against the experimental data from the tests performed at the ARA in the UK. Further papers will be published to present similar results for transonic, Mach 0.8 conditions where the dominant flow physics of interest was shock wave induced separation, as well as Reynolds number effects.

III. Review of Past Studies

The lambda wing configuration has been investigated over several decades, with research ramping up in the 1990's and early 2000's driven by the difficulties encountered with lambda wing aircraft such as the B-2 and F-117. In particular it became clear that much more research was needed to better understand the complex aerodynamics of these planforms. Experimental studies indicated that lambda wing are more susceptible to abrupt boundary layer separations and subsequent rapid stall events with unstable pitch breaks, compared with more conventional swept and tapered wings of similar sweep and aspect ratio. Boundary layer separation from the upper surface of a wing occurs firsts where the local loading is maximum. While for a swept/tapered wing, this tends to be towards the tip of the wing, it was found that with lambda wings this tended to occur much more inboard, and often around the trailing edge crank. The pitch up effect was then due to the rapid progressive development of this separation front.

The United States and United Kingdom collaborated on a number of experimental studies of lambda wings in the late 1990's. Parker et al. [1] presented results on the Model 2389, which was a wall mounted half-model with a 40^{o} leading edge sweep fixed to a simple axisymmetric body. The results of these studies, at transonic speeds, highlighted

the problem of the abrupt pitch break and studied how leading edge devices could be used to relieve the adverse pressure gradients that caused the abrupt trailing edge separations that cause these effects. At transonic speeds it was found that these separations were shock wave induced, while at low speed at high alpha, the variety of leading edge devices failed to demonstrate a significant improvement of the pitch-up problem [2]. The incipient separation at the crank was identified as a serious issue for trailing edge control effectiveness. A CFD study of this test case was performed by McParlin & Adamczak [3], employing two Reynolds Averaged Navier-Stokes (RANS) solvers using the Spalart-Allmaras and Menter SST turbulence models. They found that these models predicted the force and moment characteristics in the linear, attached flow, regime fairly well but still with significant differences between measured and computed surface pressures. At high alpha, beyond the onset of trailing edge separation, the RANS models were not able to resolve the evolving flow separations properly, but did capture occurrence of the pitch-up effect at high C_L. These and other computational studies have shown that RANS modelling with linear eddy viscosity models cannot properly capture the flow separations and subsequent stall characteristics of lambda wing configurations, and the conclusion was that higher fidelity, scale resolving unsteady methods were required to properly resolve the complex 3D flow physics involved.

Woods et al. [4] experimentally investigated a simple semi-span lambda planform model with sharp 40º swept leading and trailing edges, where leading edge separation was expected to lead to the formation of leading edge vortices. Unsteady measurements of the upper surface pressure distribution was made to map the vortex trajectory and identify vortex breakdown and the dominant buffet frequencies. Maximum buffet condition was identified as being due to vortex instability occurring between the vortex core and the primary attachment of the leading edge vortex system.

A major campaign of lambda wing research was carried out on the US developed Model 1303 configuration, which was designed by the Boeing Phantom Works on behalf of the US Air Force Research Laboratory as a generic research model. The model was specifically designed to incorporate a modular leading edge to provide experimental leading edge pressure distributions for different profiles. The results from the experimental and computational effort devoted to this model began to appear from 2006. McParlin et al. [5] focused on the effect of Reynolds number and leading edge radius on the aerodynamic performance of the Model 1303, with emphasis on the rapid stall and associated unstable pitch-up phenomena. Low speed experiments showed that the flow was sensitive to Reynolds number and that this sensitivity increased with increasing leading-edge radius. A significant computational campaign was undertaken to model the flow around the model 1303 configuration [6]-[10] which reinforced the findings that RANS based models fail to resolve accurately the complex 3D separations and subsequent stall characteristics on lambda wing configurations, as well as the Reynolds number sensitivity observed in the experimental tests involving three-dimensional swept boundary layer transition.

More recently a NATO AVT study involving the SACCON (Stability and Control Configuration) 53º swept leading edge geometry, was undertaken. The model enabled testing with either a rounded or a sharp leading edge such that leading edge separation and subsequent leading edge vortex formation could be studied. A comprehensive database of forces and moments and surface pressures was acquired at low speed in the German-Dutch Wind Tunnel (DNW-NWB) located in Braunschweig, Germany as well as in the NASA Langley 14- by 22-Foot Subsonic Tunnel. The test campaign also involved forced oscillation experiments. The corresponding campaign of CFD prediction focused on time accurate unsteady RANS (URANS) solutions on hybrid unstructured meshes, while a limited number of Detached Eddy Simulations (DES) were also performed. Frink et al. [11] showed again that RANS based methods, including URANS, whatever turbulence model was employed, failed to accurately predict the aerodynamic characteristics of this class of configuration, with the pitching moment prediction being a particular problem even at low angles of attack. Cummings and Schütte [12] and Liersch and Huber [13] also undertook computational prediction studies for the SACCON test case and reinforced these findings. It was concluded that higher fidelity scale resolving unsteady turbulent methods, such as DES, were needed and that a further detailed campaign of study, ideally involving cryogenic testing to assess Reynolds number effects, is required to potentially achieve an acceptable quality of prediction of the complex flows on this class of configuration.

The lack of high quality experimental data across a wide range of Reynolds number, for both low speed, and high speed transonic flow, was the motivation for the present NATO AVT-298 study, along with the need to better understand both the flow physics of these complex flows, and also what computational modelling and simulation methods are needed to properly resolve them.

IV. Research Methodology

The following section describes the details of the Swept Wing Flow Test (SWIFT) configuration, the wind tunnel model and the experiments performed by ARA, as well as the details of the computational codes employed, the computational meshes and solution details involved in the numerical study.

A. The SWIFT Configuration

The generic SWIFT configuration was developed for the NATO AVT-298 study by NASA and the UK Defence Science and Technology Laboratory (DSTL), the planform details for which is presented in Fig 1. It has an inboard leading edge of 60º sweep, and an outboard leading edge with a lower 30º sweep. The root chord is approximately 1 m and has the highest thickness to chord ratio. The trailing edge sweep is ±30°either side of a blended crank, and the spanwise twist washes out towards the tip. The configuration has an aspect ratio of 3.7, and more detailed geometry of the model will be presented in reference [17]. The planform layout in Fig 1, which is shown for only half the configuration, also shows the location of embedded surface pressure sensors.

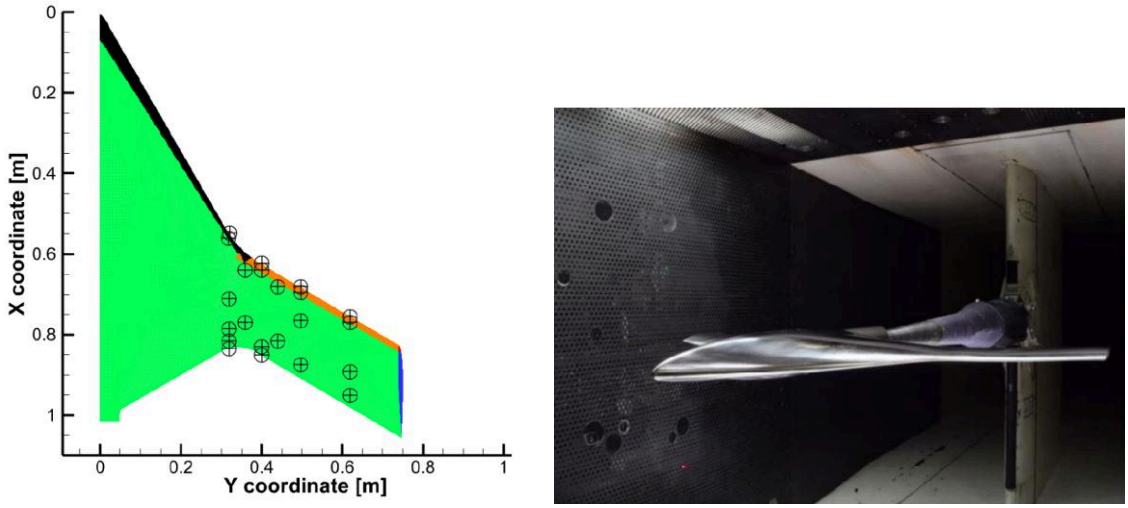

Fig. 1 The SWIFT model planform and photograph of model in the ARA Transonic Wind Tunnel.

B. Experimental Details: The ARA Experiments

Experimental campaigns have been conducted in both the Aircraft Research Association Transonic Wind Tunnel in the UK, and in the NASA National Transonic Facility (NTF) cryogenic wind tunnel in the USA. Results presented in this paper, however, focus only on comparisons against the low speed Mach 0.2, 2.5 million Reynolds number data acquired in the ARA facility. Fig 1 presents a photograph of the SWIFT model mounted in the ARA Transonic Tunnel from its sword/sting system.

The ARA Transonic Wind Tunnel is a closed circuit continuous flow tunnel with a 9 foot wide x 8 foot high x 12 foot long (1.74m x 2.44m x 3.66m) working section with perforated side walls of 22% maximum porosity. The tunnel operates at one atmosphere, with the ability to vary stagnation pressure by ±0.2 bar, across a Mach number range from low speed up to Mach 1.4. This allows of testing in the Reynolds number range of 3.5 to 16.7 million per metre.

The SWIFT model was designed to fit an internal strain gauge balance with the facility to fit sealed heated bays for instrumentation when installed in the cryogenic test facility in NASA Langley, and was manufactured by ARA from maraging steel for low temperature testing. The modular structural design allowed for the embedding of a number of static pressure taps and some kulite pressure sensors for acquisition of high frequency pressure fluctuation data. Details of these are provided in the project final technical report [17]. The model was mounted from a rear sting support allowing pitching in the range -10º to +40º, and the measurement of 6-components of force/moments. The reference length for the pitching moment coefficient calculation was taken as the balance center location of $x_m = 0.603$ m.

Various tests were performed at Mach numbers from 0.2 (the focus of the present paper) up to Mach 0.8, involving pitch-pause α sweeps at a limited number of Reynolds number conditions, and boundary layer transition tripping. The conditions investigated in this paper include the fully turbulent case with transition fixing at the leading edge, and a

condition where transition was fixed at 15% *x/c* along the span of the model upper and lower surface, for the *M*=0.2, $Re\bar{c}$ (based on mean chord, $\bar{c}$ of 559.1 mm) of 2.5 million.

The NASA NTF tests employed a subsonic transition fixing strategy to match an expected full scale aircraft case, termed ST2, which was devised during the course of the study, the details of which are reported in the project final report [17], but the laminar flow zones on the upper surface are depicted in the planform image of Fig 1 as the black (inboard) and orange (outboard) areas. The lower surface transition lines were calculated to be different but similar to the upper surface shown here. All of the CFD modelling and simulation undertaken and presented in this paper, for the aft subsonic transition fixing cases, were for the ST2 configuration and not for the ARA 15% *x/c*, so direct comparison of the CFD and the ARA experimental data for the transition fixing cases are not strictly valid. However the two transition strategies were not so different that the overall lift and drag characteristics were expected to be significantly different, and this was found to be the case when the recent comparisons between the two sets of experimental data have been made – the NASA test data not having been made available when the comparative analysis was performed for this paper.

C. Computational Modelling and Simulation

Several computational prediction approaches, encompassing two separate computer codes, were employed on the analysis of these flows in order to assess the accuracy, across the pitch range, of these modelling and simulation approaches to capture the complex flow physics, thereby identifying the most accurate approach and the key differences between them. The two codes employed were, i) the Viscous Full Potential code (VFP) and ii) the FLUENT commercial CFD code, the details of which are here presented.

The Viscous Full Potential (VFP) Code

The VFP code solves the coupled inviscid full potential equations and 2D integral boundary layer equations which are extended to account for spanwise flow component in swept wing boundary layers. For transonic cruise the shock waves over wings and bodies are relatively weak, and the rise in entropy associated with these is small enough to consider the flow to be isentropic with negligible error in the calculation of pressure and velocity. Consequently, the full (non-linear) potential flow equations, which are obtained from reducing the Navier-Stokes equations by neglecting viscosity and assuming the flow to be isentropic and irrotational, are entirely consistent with the desired flow characteristics for transonic cruise. The full velocity potential equation, for an irrotational, inviscid, isentropic flow, in terms of Cartesian coordinates (*x,y,z*) is given as:

$$\left(1-\frac{\bar{\Phi}_x^2}{a^2}\right)\bar{\Phi}_{xx}+\left(1-\frac{\bar{\Phi}_y^2}{a^2}\right)\bar{\Phi}_{yy}+\left(1-\frac{\bar{\Phi}_z^2}{a^2}\right)\bar{\Phi}_{zz}-2\frac{\bar{\Phi}_x\bar{\Phi}_y}{a^2}\bar{\Phi}_{xy}-2\frac{\bar{\Phi}_x\bar{\Phi}_z}{a^2}\bar{\Phi}_{xz}-2\frac{\bar{\Phi}_y\bar{\Phi}_z}{a^2}\bar{\Phi}_{yz}$$

$$-2\bar{\Phi}_x\bar{\Phi}_{xt}-2\bar{\Phi}_y\bar{\Phi}_{yt}-2\bar{\Phi}_z\bar{\Phi}_{zt}-\bar{\Phi}_{tt}=0 \tag{1}$$

where the velocity potential Φ is defined by:

$$V=\sqrt{u^2+v^2+w^2} \;=\; \nabla\bar{\Phi} \tag{2}$$

such that:

$$u=\bar{\Phi}_x=\frac{\partial\bar{\Phi}}{\partial x}, \qquad v=\bar{\Phi}_y=\frac{\partial\bar{\Phi}}{\partial y}, \qquad w=\bar{\Phi}_z=\frac{\partial\bar{\Phi}}{\partial z} \tag{3}$$

and the time, *t*, is in the unsteady terms. If the flow is steady, the last four terms of the equation are neglected, as is the case in the calculations presented in this paper. The viscous boundary layer can be modelled by solving the 3D integral boundary layer equations. For simplicity the 2D integral boundary layer equations are given here for illustrative purposes. The boundary layer momentum equation is given as:

$$\frac{d\theta}{dx} = \frac{C_f}{2} - \frac{\theta}{U_e}\frac{dU_e}{dx}(H - 2 - M_e^2) \tag{4}$$

and is solved together with an auxiliary equation, called the entrainment equation, which describes the inflow of external air into the boundary layer as it thickens in the streamwise direction, typically given as:

$$\frac{d(\delta - \delta^*)}{dx} = C_E - \frac{\delta - \delta^*}{U_e}\frac{dU_e}{dx}(1 - M_e^2) \tag{5}$$

where C_E is the entrainment coefficient, which is a function of the boundary layer shape factor, $H = \delta^* / \theta$. The terms U_e and M_e are the streamwise velocity component and corresponding Mach number at the top edge of the boundary layer, and the boundary layer displacement thickness, δ^*, and momentum thickness, θ, are defined as:

$$\theta = \int_0^{\delta} \frac{\rho U}{\rho_e U_e}\left(1 - \frac{U}{U_e}\right) d\xi \tag{6}$$

$$\delta^* = \int_0^{\delta} \left(1 - \frac{\rho U}{\rho_e U_e}\right) d\xi \tag{7}$$

where ξ is the wall normal dimension.

The three-dimensional integral boundary layer equations and their solution for straight, swept and tapered wing flows, and their solution are given by Smith [14]. The VFP code, used here, is described in reference [15] and was created specifically for analysis of transonic cruise aircraft configurations, including conventional swept wing / body configuration, as well as blended wing configurations. The code uses a relaxation algorithm to solve the finite difference form of the full three-dimensional velocity-potential equations which are coupled with the semi-inverse, swept / tapered integral boundary layer method of Ashill and Smith [16]. The boundary layer displacement thickness obtained from the boundary layer solver was then used to update the surface shape by the addition of the resulting displacement thickness distribution before another FP calculation was performed on the updated surface geometry. The convergence criteria was set as a maximum absolute change in value of velocity perturbation potential anywhere in the flow, reduced to an order of 10^{-6}. The structured meshes, generated automatically by the code, comprised 135,432 cells, which in past studies have been found to be sufficient for this class of configuration.

The FLUENT CFD Code

The FLUENT commercial flow solver allows the computation of the Navier-Stokes equations for compressible, unsteady, viscous laminar and turbulent flow by either modelling approaches (Reynolds averaging via a turbulence model) or feature resolving simulation (time accurate Delayed Detached Eddy or Large Eddy simulation). The calculations for this paper employed the Roe approximate Riemann solver for shock capturing, with a second order scheme in both space and time to obtain converged steady flow solutions as starting solutions for unsteady Delayed Detached Eddy Simulation (DDES).

A number of turbulence models were tested in this study, including the Spalart-Allmaras turbulence model with curvature corrections and a version of the quadratic constitutive relations (RC-QCR2000), the k-ω SST model of Menter and the Realizable k-ε turbulence model. All of the DDES simulations, however, used only the Spalart-Allmaras model described above, for the near wall treatment. For modelling the ST2 transition case, a zonal approach was employed whereby cells within 3D cylindrical zones surrounding the laminar flow regions around the leading edge were "tagged" such that the turbulence equations could be switched off in these zones. In this, primitive manner, the effects of transition were assumed to occur with an abrupt transition event along the prescribed ST2 transition lines. For the DDES calculations, a time step of 1 millisecond was used with a maximum of 50 iterations per time-step. The convergence criteria for the calculations was overall force coefficient convergence to three significant figures together with residual convergence to at least 10^{-4}.

A flow domain with a symmetry boundary condition along the model symmetry plane was constructed, on the basis that the flowfield, within the angle of attack range of interest, was assumed to be symmetric about this plane. The spherical outer boundary (pressure farfield boundary condition) was located at 50x the model span away from the

nose reference point. The NTF sting structure, similar to that used in the ARA test, was modelled in order to resolve the sting-model interference effects at high angle of attack, negating the need for corrections for this effect.

Hybrid unstructured meshes were employed with prismatic embedded cells grown out from the wall surfaces, whereby the boundary layers were captured within 30 – 40 cell layers, and with the first cell height set at 5.6×10^{-6}m, which was obtained using a turbulent Blasius approach to give values of y+ of the order of 1.0 close to the nose of the configuration. A mesh sensitivity analysis was performed for the α=5° test case that showed that a mesh of 27.9 million cells, shown in Fig 2, was sufficient to resolve the forces and moments to three significant figures with no discernable differences in surface pressure comparisons along the wing.

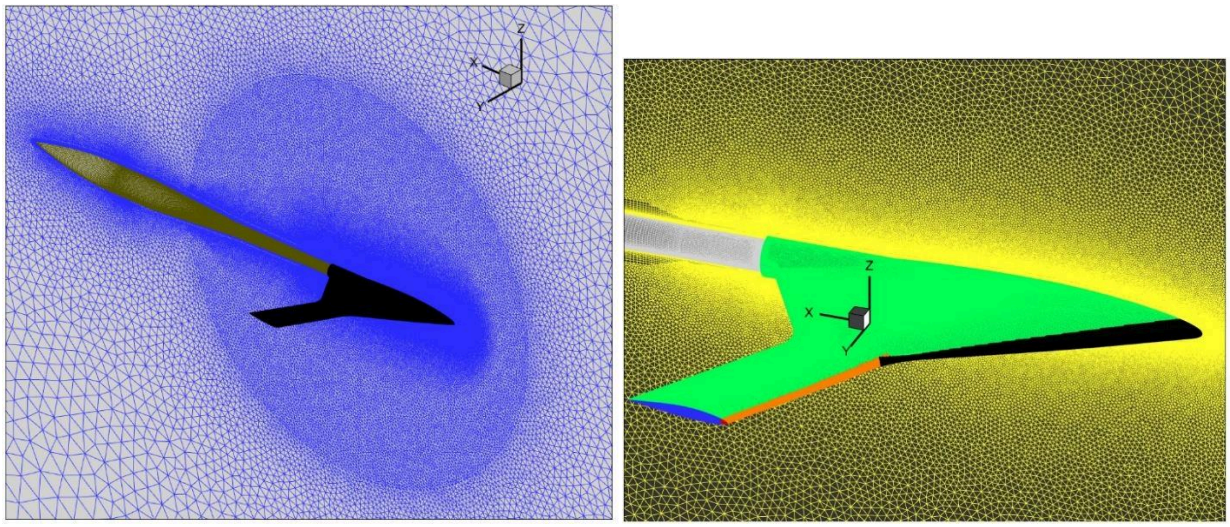

a) Full view of the half-span mesh

b) Focused view on the model surface with laminar leading edge zones (black and orange) according to the ST2 transition fix configuration

Fig. 2 The computational mesh.

V. Results and Discussion

This section compares the results from the ARA experiments and the numerical results from the VFP analysis and from the RANS and DDES analysis of Mach 0.2, 2.5 million Reynolds number test cases of this study. A future paper will present a similar comparison for the transonic Mach 0.8 cases.

A. Comparison of Forces and Moments

Figs 3 – 6 present comparisons of the measured experimental data for overall forces and moments acquired in the ARA Transonic Wind Tunnel, and those predicted using the VFP method (up to predicted boundary layer separation onset, when the code becomes invalid and fails to converge for higher α) and the FLUENT code for various modelling and simulation approaches. The first plots a) compare the results for the steady flow methods (fully turbulent RANS with various turbulence models, and VFP along with the result for the ST2 transition case using the Spalart-Allmaras model) while plots b) present the corresponding comparisons for URANS and DDES unsteady flow methods for the two boundary layer cases – fully turbulent and ST2 transition cases, where the data is time averaged. Plots c) plot the same data in the higher α range and include the bounds for maximum and minimum values recorded over the computed time period of ~0.5 seconds of statistically converged flow time.

Fig 3 presents the comparison of C_L versus α for the various modelling and simulation methods. The comparison of the steady flow methods show that all these methods agree closely with the experimentally measured lift curve with the VFP result slightly underpredicting at the higher α range, within 2% of the measured figure, while the RANS results were within ~1% up to α=10°, where the VFP code would not converge, indicating the detection of incipient trailing edge separation. In the non-linear region the k-ω SST turbulence model was found to be the superior of those tested, following the experimental data up to α=14° before predicting an abrupt stall event. The experimental data does not exhibit evidence of any stall event, however. The other two fully turbulent RANS results predict a stall even

at a lower α = 12°, the Realizable k-ε model predicting a much more severe post-stall lift loss. Introducing the ST2 forced transition model, with laminar flow along the leading edge region gives the onset of non-linear lift at α=10°, a stall event at 12° and a recovery in the post stall lift trend. Comparing the unsteady methods in Fig 3b) for the two turbulence cases, the DDES results clearly follow the experimental lift trend much better than the unsteady RANS results. The fully turbulent DDES prediction shows a stall event at α=14° followed by a recovery, while the corresponding DDES result with the ST2 transition line modelled does not capture a stall event at all, up to α=15°, which better agrees with experimental data. The URANS results follow almost the same trend as the equivalent steady RANS result. Plotting the maximum and minimum values of C_L, resolved in the unsteady ST2 transition predictions, over a 0.5 second period of statistically stabilized simulation reveals that in both URANS and DDES cases, the level of fluctuation in lift increased with α, as expected. Interestingly, the minimum C_L seen in the DDES was always higher than the maximum C_L predicted by the URANS method.

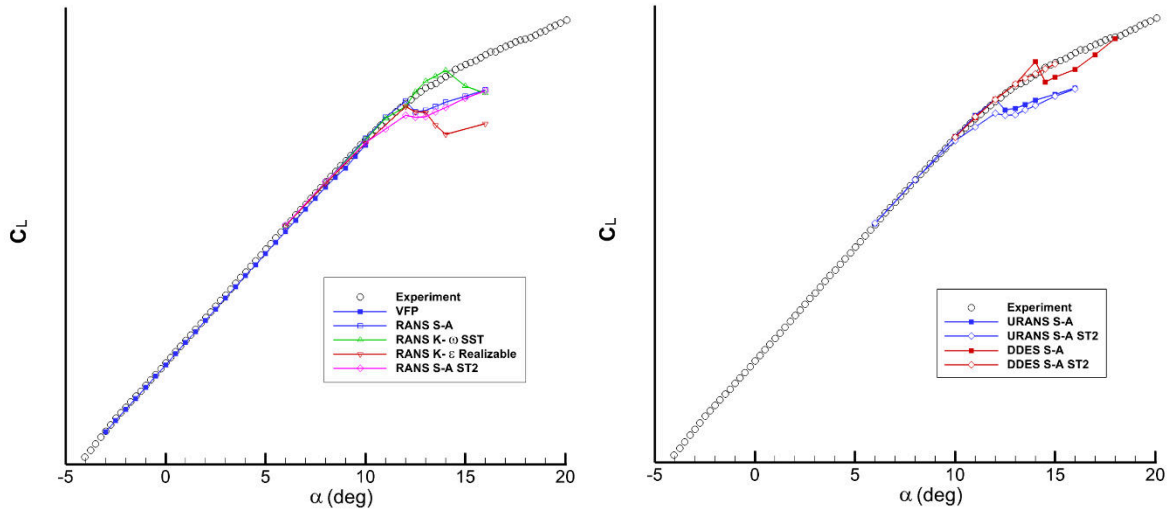

a) Steady flow methods **b) Unsteady flow methods**

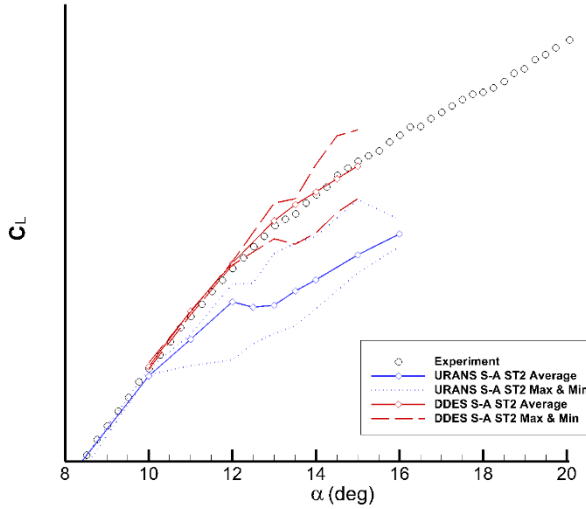

c) Average C_L and maximum and minimum bounds for the unsteady flow ST2 case

Fig. 3: Comparison of C_L versus α for the various CFD methods assessed. M = 0.2, $Re\bar{c}$ = 2.5 x 10^6.

The corresponding plots for the drag coefficient are presented in fig 4. The VFP code is seen to have predicted the drag trend remarkably well for a lower order method, with almost equivalent values compared with experiment at zero

α, to a 15% over-prediction at $\alpha = 10^o$. In fact the fully turbulent RANS results overpredict the C_D even more than the VFP method from – by up to 20%. The best match is achieved by the ST2 RANS result which makes sense, as the ARA experiment employed a transition trip strategy similar to the ST2 shape, such that C_D levels would be expected to be slightly lower than a fully turbulent leading edge case. Scrutiny of the unsteady predictions show, again, that for C_D the DDES method is superior to the URANS method in capturing the experimentally measured drag trend. The experiment gives a drag rise occurring between $\alpha = 13^o$ and 14^o, while the fully turbulent DDES result predicts this as happening late, at $\alpha \sim 14^o$. The ST2 transition prediction, meanwhile, captured a premature drag rise at $\alpha = 12\text{-}13^o$. This event will be extremely sensitive to the upper surface transition line, and so this result is not surprising given that the ARA transition was closer to the leading edge on the inboard wing. The URANS calculations predicted drag rise to occur at much lower α, clearly indicating this method's inability to capture the correct physical trends. Looking at the maximum and minimum C_D bounds detected in the unsteady calculations for the ST2 transition cases, reveals a much higher range of fluctuating C_D in the URANS result compared with the DDES result, indicative of much more extensive separated flow regions predicted in the former result. Unsteadiness in the DDES resolved drag prediction is not significant until between $\alpha \sim 13^o$, whereas significant unsteadiness is predicted in the URANS predicted flowfield even at $\alpha = 8^o$.

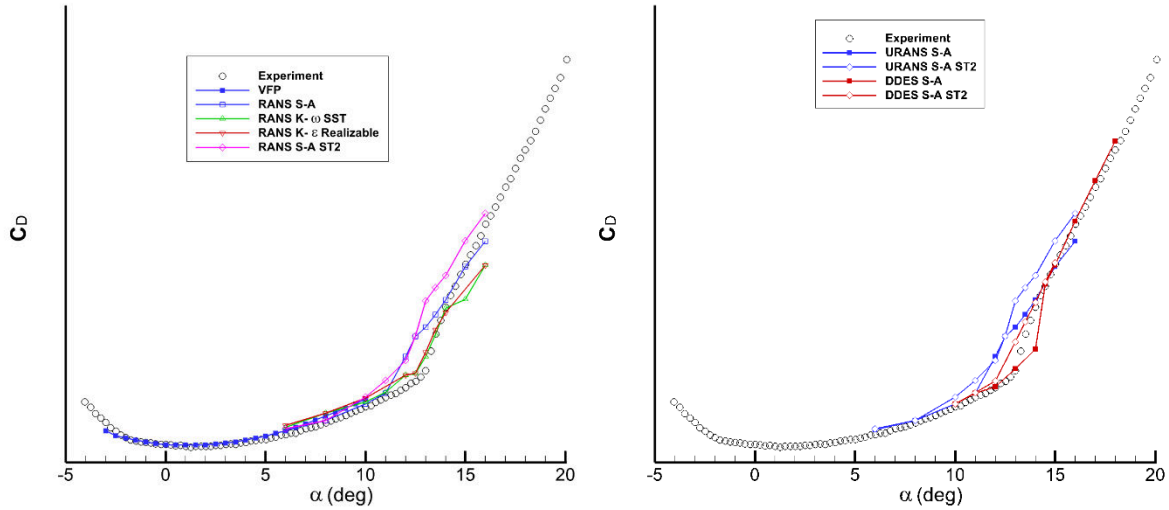

a) Steady flow methods **b) Unsteady flow methods**

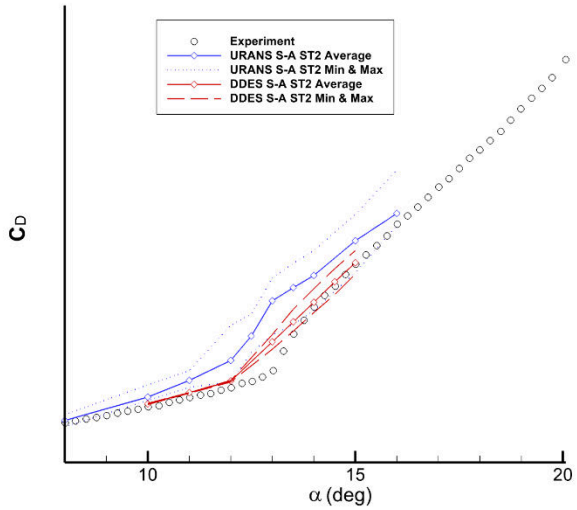

c) Average C_D and maximum and minimum bounds for the unsteady flow ST2 case

Fig. 4: Comparison of C_L versus α for the various CFD methods assessed. M = 0.2, $Re\bar{c}$ = 2.5 x 10^6.

Fig 5 presents the corresponding comparisons for pitching moment about the reference point on the body centreline, 0.603 m from the model nose. It should be noted that the values of C_M are very small since this reference point is very close to the model centre of pressure. As a result, the confidence levels in the magnitude of C_M are likely to be relatively low. Results for the higher fidelity CFD methods are not available for the very lowest angles of attack, where the VFP result is underpredicted by as much as $\Delta C_M \sim 0.004$. This is actually not a bad result for a lower fidelity method which can produce a data point in a small fraction of the time needed for a RANS result. The Spalart-Allmaras and k-ω SST models predict the pitching moment relatively well up to about 11° angle of attack beyond which they correctly predict the pitch up trend seen in the experiment, but not the recovery in pitching moment seen in the experimental data at around $\alpha = 13°$, before the trend continues. None of the steady flow methods predict this reversal in the C_M trend. The Realizable k-ε model over predicts C_M between $\alpha = 6° - 12°$, followed by a large divergence which is also seen in the Spalart-Allmaras ST2 transition result. The closest match with experiment is achieved with the fully turbulent DDES method, which was the only method that resolved the C_M reversal feature seen in the experimental data.

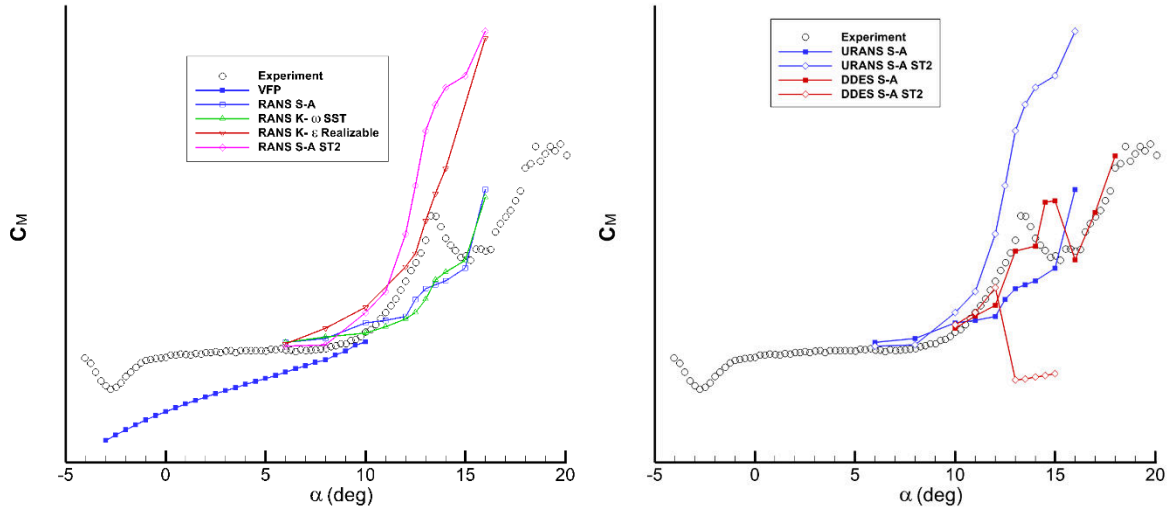

a) Steady flow methods **b) Unsteady flow methods**

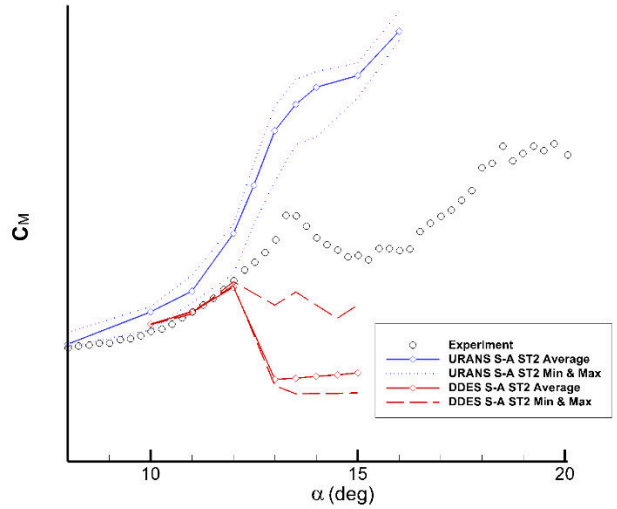

c) Average C_M and maximum and minimum bounds for the unsteady flow ST2 case

Fig 5: Comparison of C_M versus α for the various CFD methods assessed. M = 0.2, $Re\bar{c}$ = 2.5 x 10^6.

The other unsteady predictions were found to be no better than the steady RANS results. The unsteady ST2 results predicted opposite post trailing edge separation trends – the URANS result predicting increasingly positive C_M, while the DDES result predicting a drop in C_M to near zero, with more unsteadiness in the pitching moment found in the DDES data.

Fig 6 compares the results for lift to drag ratio – a measure of the aerodynamic efficiency of the SWIFT lambda wing model. Again the VFP method is seen to provide a remarkably accurate prediction up to α = ~4°, correctly resolving peak *L/D* at around α = 7°, although this is underpredicted by ~8% - still a remarkably good result. The steady RANS predictions all correctly resolve the trend seen in experiment but tend to capture peak efficiency at a few degrees higher than experiment, and the variation in the curves makes it difficult to identify a clear winner in best predicting the experimental trend. From the comparisons of the unsteady methods, the DDES results better match the experimental data, with the ST2 result best matching the post-separation trend. Interestingly the DDES predictions do not indicate significant fluctuation in the *L/D* parameter, unlike the URANS predictions.

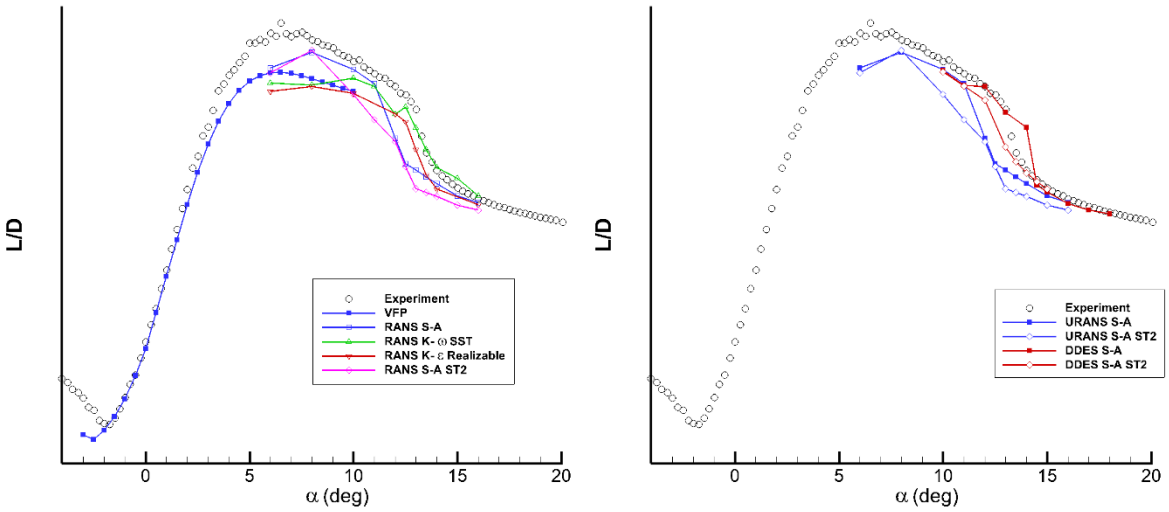

a) Steady flow methods **b) Unsteady flow methods**

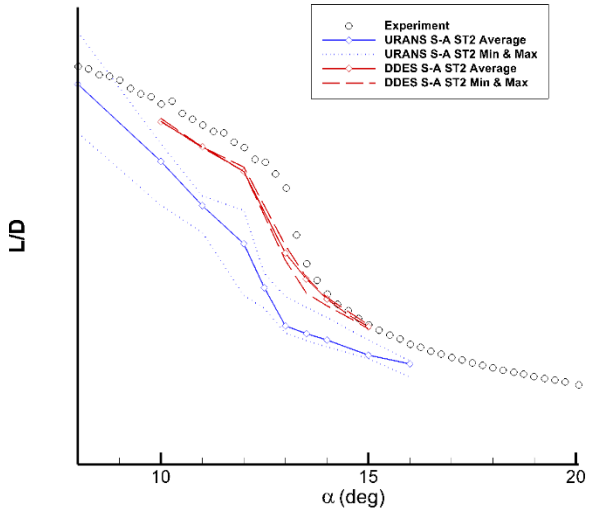

c) Average *L/D* ratio and maximum and minimum bounds for the unsteady flow ST2 case

Fig 6: Comparison of *L/D* ratio versus *a* for the various CFD methods assessed. M = 0.2, $Re\bar{c}$ = 2.5 x 10^6.

B. Comparison of Surface Pressure Distributions

Comparisons of experimentally measured and CFD computed surface pressure distributions at three spanwise sections are presented for $\alpha = 8^o$ and 14^o in Figs 7 and 8 respectively. For the lower angle of attack case, presented in Fig 7, only the steady flow results are plotted as the time averaged unsteady flow data are equivalent to the Spalart-Allmaras results shown here, since there is no flow separation at this angle of attack, and consequently the flow is quasi-steady. For the α=14^o case these comparisons also include instantaneous C_p distributions obtained from the unsteady methods for an instant where C_L is at its time averaged value. All methods successfully capture the C_p distributions at all three spanwise stations very well, the only difference being the VFP prediction at the trailing edge. The real geometry had a slightly blunted trailing edge, which was correctly modelled in the CFD mesh. The VFP code, however, requires a sharp trailing edge for numerical stability, which is the reason for the predicted divergence in pressure at the trailing edge.

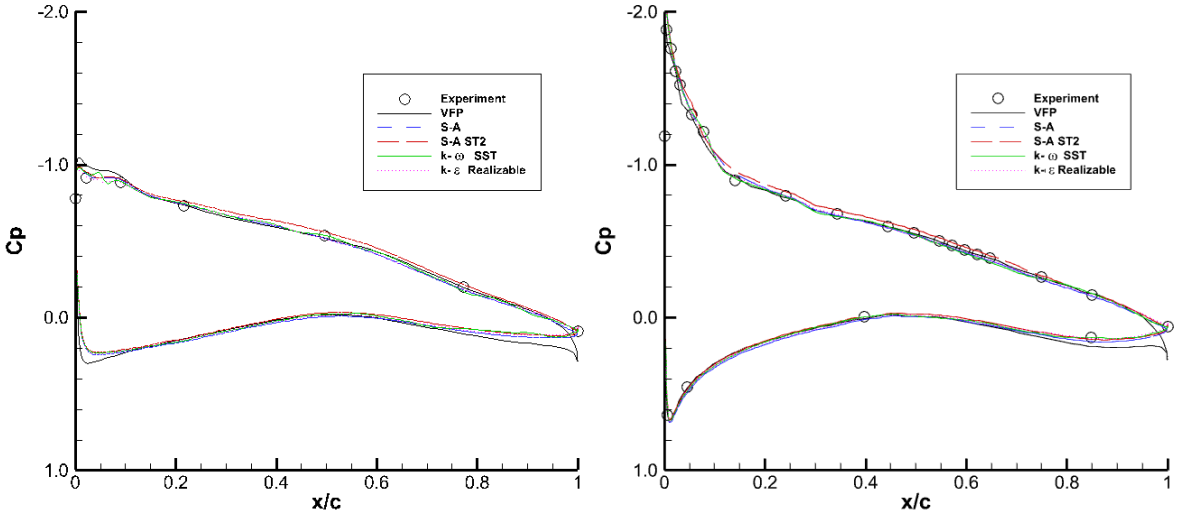

a) y = 301.5 mm **b) y = 382.5 mm**

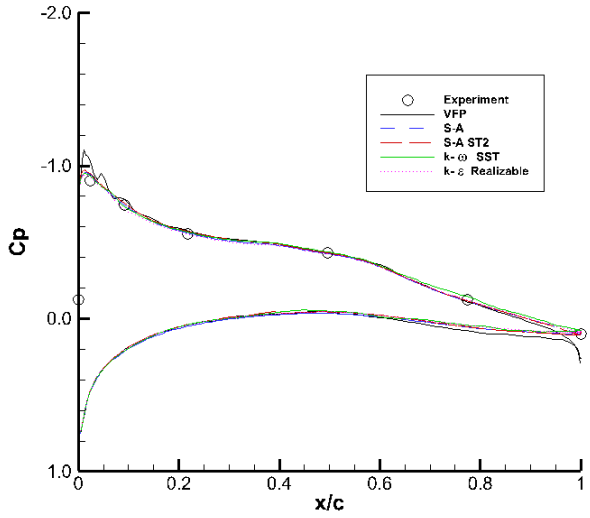

c) y = 606 mm

Fig 7: Comparison of surface Cp distribution for the various CFD methods assessed. M = 0.2, a = 8^o, $Re\bar{c}$ = 2.5 x 10^6.

The comparisons for the higher 14^o angle of attack case are plotted in Fig 8, where representative instantaneous C_p distributions are presented for the unsteady methods (Figs 8b) and c)), to highlight the chaotic nature of the flow in the centre-span region where the trailing edge separation begins (as opposed to tip separation in the case of

conventional swept/tapered wings). Among the steady flow methods using linear eddy viscosity turbulence models, the clear winner in terms of the closest match with the experimentally measured time average surface pressures, is the k-ω SST turbulence model, which correctly predicts significant levels of upper surface leading edge suction, where the other models fail significantly to resolve this effect. In fact this prediction is on a par with those resulting from DDES analysis. Once the time series surface pressure data are time averaged, to match the experimental data, the ST2 DDES simulation came out best matching the experimental data, particularly in terms of the leading edge suction profile. The ST2 DDES transition cases exhibit higher levels of fluctuating upper surface pressures than seen with the fully turbulent DDES simulations.

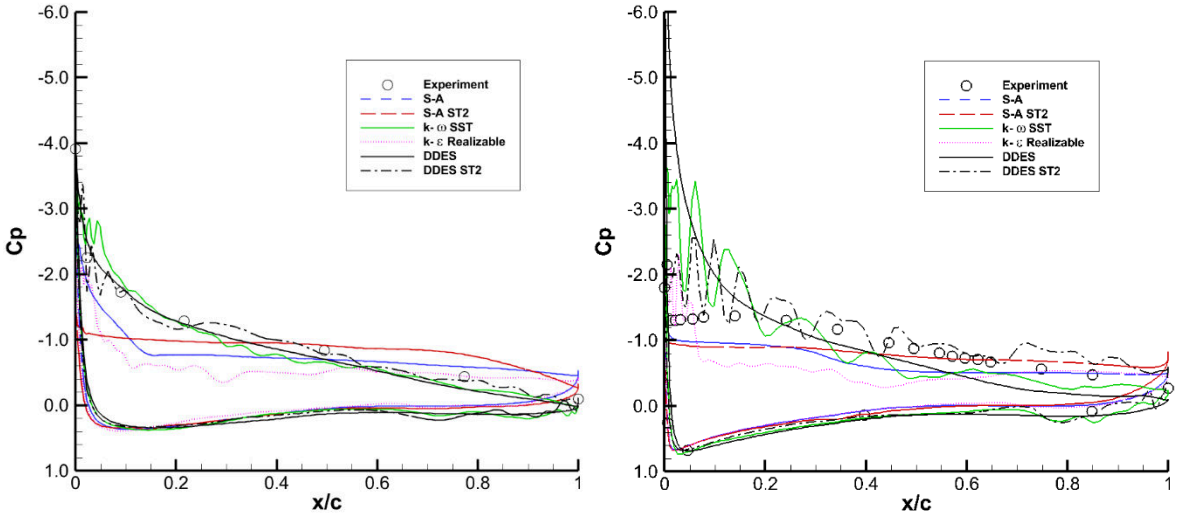

a) y = 301.5 mm **b) y = 382.5 mm**

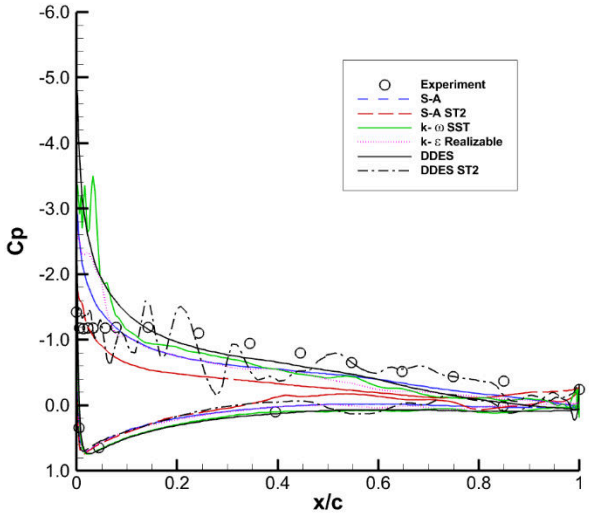

c) y = 606 mm

Fig 8: Comparison of surface Cp distribution for the various CFD methods assessed. M = 0.2, a = 14°, $Re\bar{c}$ = 2.5 x 10^6.

C. Flow Field Visualization

Figs 9 to 11 present sample flow field visualization images highlighting the considerable differences between the steady time averaged results provided by RANS (Spalart-Allmaras with QCR correction) and by the corresponding Delayed Detached Eddy simulation solution, for the same time averaged C_L condition in both cases. Fig 9 presents the comparison between instantaneous contours of velocity magnitude at a crossflow plane at y = 342 mm, at α = 14°, and

demonstrates the very large difference in the flowfields in this location. The RANS solution predicts a very large separation emanating from the leading edge of the wing, akin to a quasi 2D wing in deep stall condition. The instantaneous flow field resolved using DDES (in this case fully turbulent) exhibits much finer detail, capturing individual large eddies / turbulent coherent structures emanating from the separation front near the leading edge and convecting downstream. The region of viscous flow is seen to be significantly smaller, with a significant region of accelerated flow over the leading edge which simply does not exist in the RANS solution. Plotting the time averaged velocity contours for both computational cases reveals that the DDES flowfield at this spanwise location is very different to that resolved using RANS. Since this study, and many others, has shown that scale resolving simulation is far superior in correctly resolving the detailed physics of separated flowfields, the implications of RANS solutions yielding very different time averaged flowfields to those predicted by DDES is potentially very serious. This suggests that RANS modelling cannot be relied upon to correctly predict the non-linear aerodynamics of wing flows, or indeed any heavily separated flows.

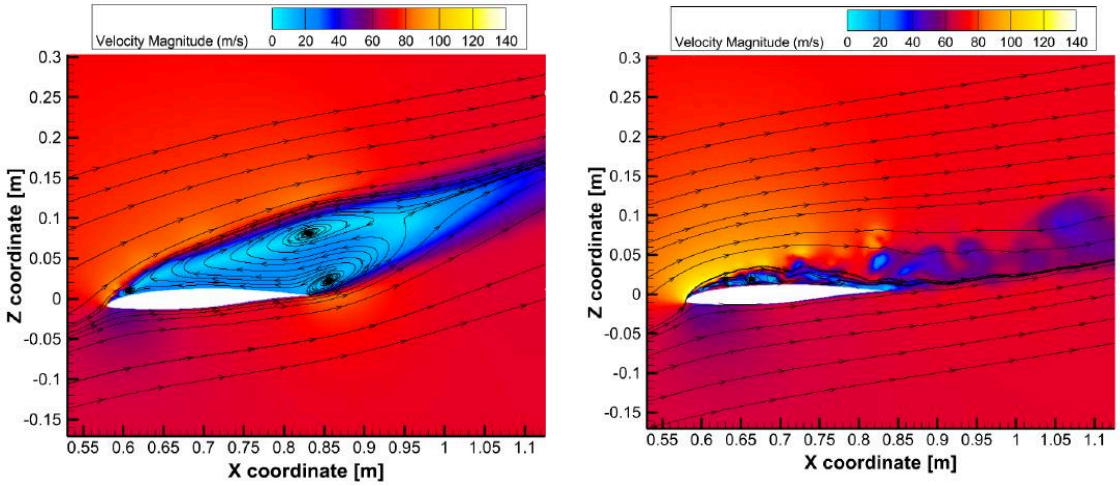

a) RANS (S-A) **b) DDES (S-A)**

Fig 9: Predicted instantaneous velocity contours in a spanwise cut at $C_{L(average)}$ condition, y = 342mm, $\alpha = 14^o$. $M = 0.2$, $a = 14^o$, $Re\bar{c} = 2.5 \times 10^6$.

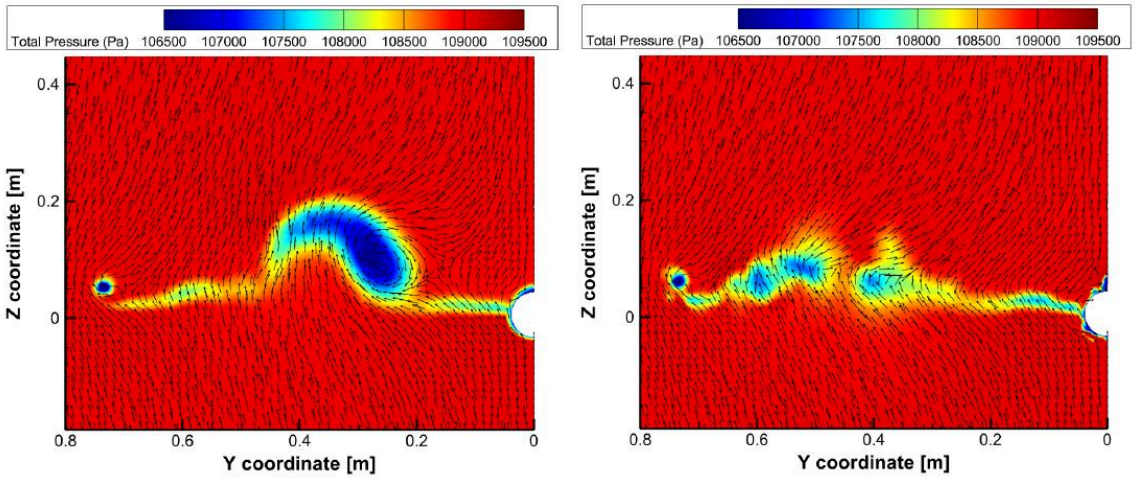

a) RANS (S-A) **b) DDES (S-A)**

Fig 10: Predicted instantaneous velocity vectors and total pressure contours in crossflow plane at x=1155mm at $C_{L(average)}$ condition, $a = 14^o$. $M = 0.2$, $a = 14^o$, $Re\bar{c} = 2.5 \times 10^6$.

This is also demonstrated when considering the structure of the viscous wake downstream of the wing. Fig 10 presents instantaneous velocity contour and flow vectors in a crossflow plane at x = 1155mm, for the $\alpha = 14^o$ case.

The RANS result resolves the small wing tip vortex that appears at y ~ 750mm, but the dominant feature is a large vortex and its severed feeding shear layer emanating from the crank region of the trailing edge, which does not exist to the same extent in the instantaneous flowfield resolved in the DDES simulation. This issue in RANS capturing the wrong separated flow field is further highlighted in Fig 11, which plots the wake flowfield as contours of Q-criteria.

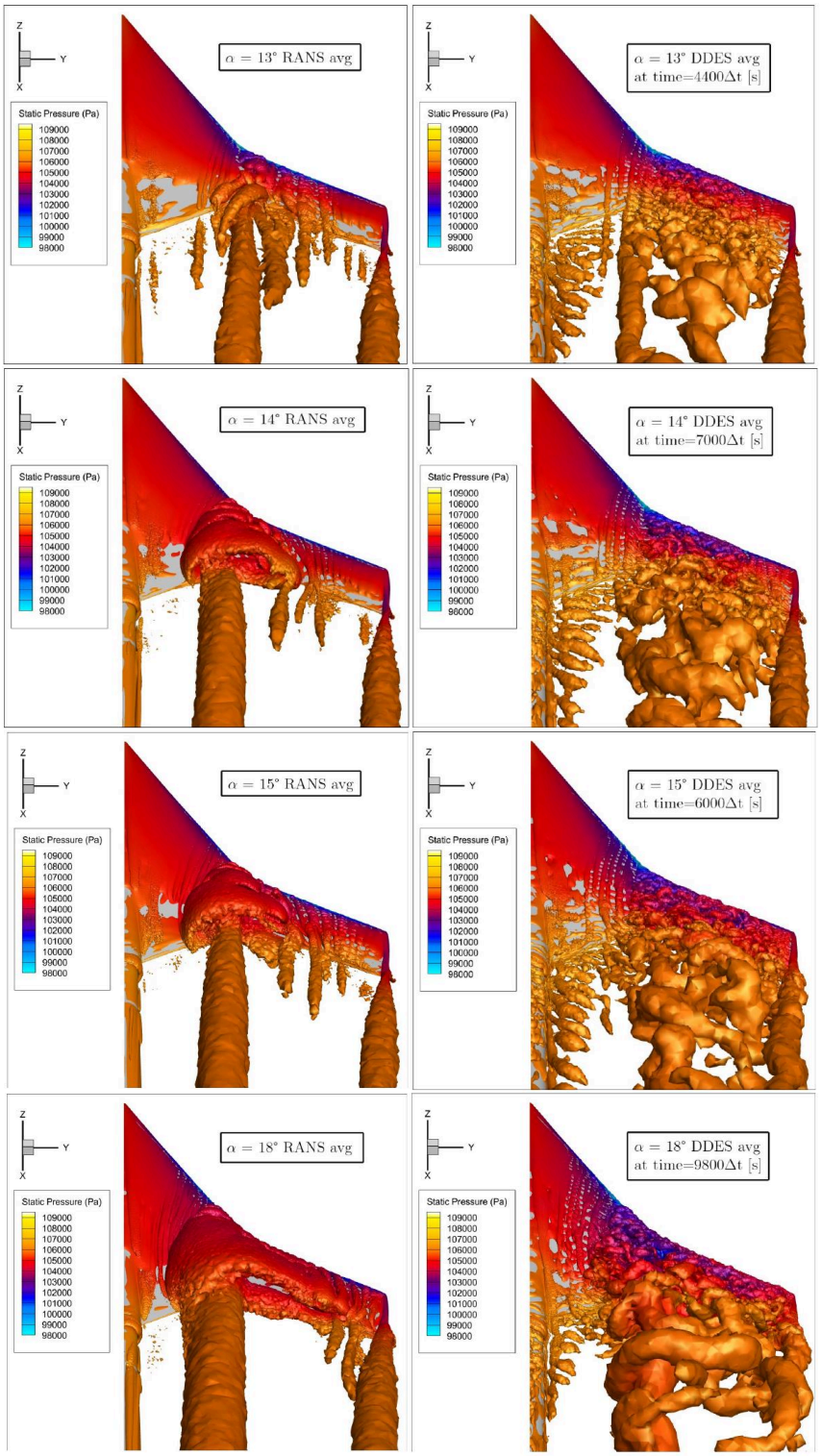

Fig 11: Comparison of the predicted Q-criterion iso-surface (Q=20,000 flooded by static pressure contours) for the flow over the upper surface at the $C_{L(average)}$ condition. M = 0.2, a = 13°-18°, $Re\bar{c}$ = 2.5 x 10^6.

Here the predicted instantaneous wake flowfield at the same averaged C_L condition is presented in terms of calculated Q criterion set to a suitable magnitude to highlight dominant vortical structures, for several angles of attack at which the flow is highly separated. The resolved flow structured predicted by the RANS model is seen to be significantly different that resolved by the DDES method, which captures much more fine detail of the different scales of vortical structures not seen in the RANS solution. The very structured separation mechanism identified in the RANS solution is very different, and almost certainly wrong, in comparison to that predicted by the DDES solution. In particular the DDES simulation does not resolve the strong coherent streamwise vortex that is resolved in the RANS solution.

D. **Unsteady Pressure Fluctuations**

Fig 12 presents selected data from the analysis of the time series of the static surface pressure acquired in the DDES simulations, which will allow for a direct comparison with those acquired in the experiments. The data is presented as single-sided (real component) Fast-Fourier Transform (FFT) spectra of the pressure fluctuations against the Strouhal number (St) over a 0.5 second time series for the sensor stations 1, 2, 3, 4, 9 and 20 on the inboard spanwise section of the wing. Although the time step in DDES simulations is relatively high (1 millisecond) the data captured indicates vortex shedding frequencies have been captured well at the aforementioned stations. This is in line with the visual representation of large vortex in Fig 11. DDES has been successful in capturing energy containing frequencies however the dissipation of energy seems not to follow the $k^{-3/2}$ slope, as hypothesized by the Kolmogorov theorem, in most of the spectra plots below except for the station 2. As the station 2 is much closer to the leading edge the mesh resolution in this area is relatively very high compared to other stations resulting in better capture of shedding frequency as well as dispersion closer to the $k^{-3/2}$ slope in energy spectra. On the other hand, the station 1, although still within the highly refined mesh region at the leading edge, does not exhibit similar vortex shedding trend. At almost all the stations, except the station 2, the dissipation of energy is almost exponential which could be due to two major factors namely the large time step and lack of mesh resolution in those regions.

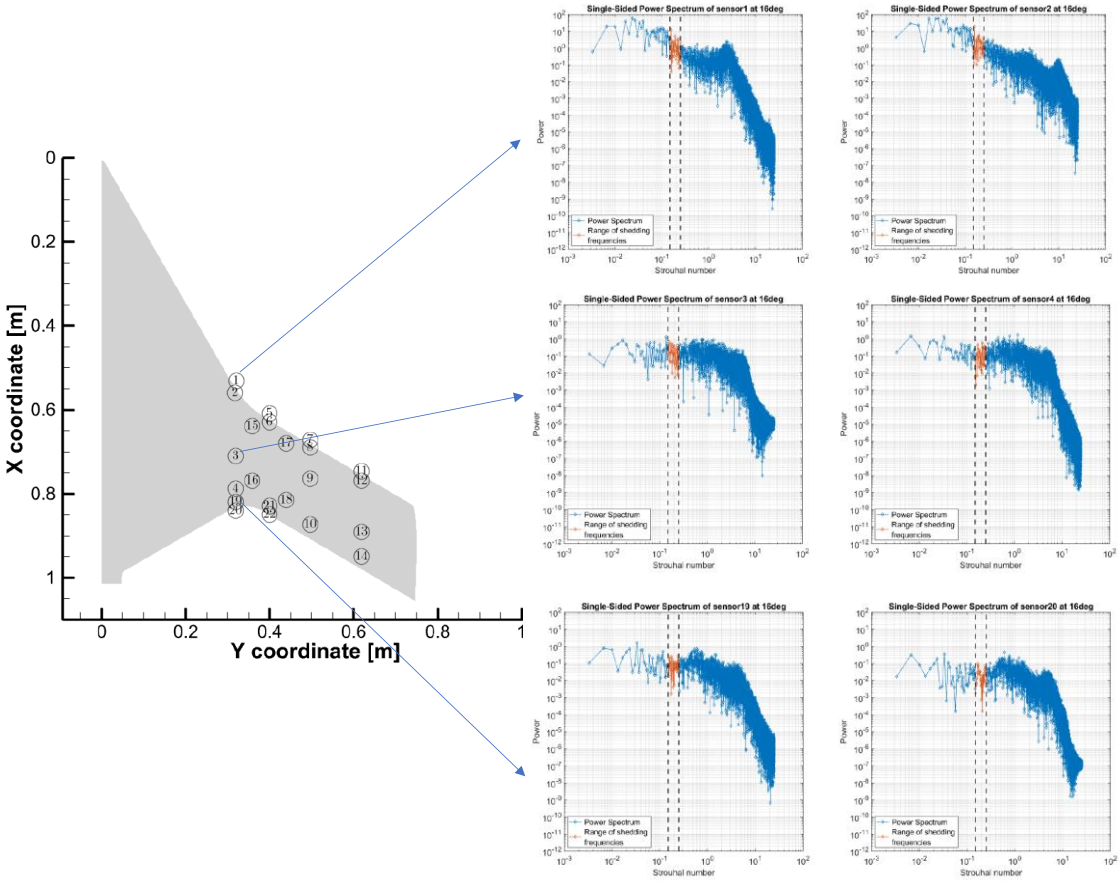

Fig 12: FFT spectra of the pressure fluctuations from six virtual kulite sensors. DDES simulation, M = 0.2, a = 16°, $Re\bar{c}$ = 2.5 x 10^6.

VI. Conclusions

Computational aerodynamics analysis on the SWIFT Lambda configuration at subsonic airspeed of Mach 0.2 have been presented in this article which was undertaken as part of the NASA AVT-298 Task Group to investigate the effects of Reynolds number scaling on swept wing flows. The current study, presented at fixed Reynolds number of 2.5 million, presents investigations for which experiments were conducted at the ARA transonic wind tunnel in the UK. The study has been conducted at the pitch sweep from -4 to 20 degrees angles of attack using various CFD frameworks including steady RANS, Unsteady RANS, DDES and lower fidelity Viscous Full Potential (VFP) methods which highlight the complex 3D stall initiating inboard which is different from that seen on a conventional swept, tapered wings in civilian aircrafts. Various turbulence models have been employed to verify the calculations against the experimental data and it has been observed that the k-ω SST turbulence model has performed much better than its other competitors however at higher angles of attack even the k-ω SST turbulence model was not able to match the experimental data and underpredicted or even provided wrong predictions. The VFP method has shown promising predictions, however again only at lower angles of attack as the it can be observed that it underpredicted at higher angles of attack, as anticipated. On the other hand, the DDES framework performed slightly better than RANS frameworks due to its higher fidelity nature. DDES highly depends upon the mesh resolution near the wall and the employed timestep. Although very good prediction has been observed for the given timestep of 1 millisecond, however with even smaller timestep better flow predictions can be expected especially in the energy spectrum. It is safe to conclude that for this particular case perhaps the eddy viscosity based models are unsuitable and a higher fidelity method such as Large Eddy Simulations (LES) or Implicit Large Eddy Simulations (ILES) could be better candidates due the superior performance of these frameworks for near wall flows.

Acknowledgments

The authors acknowledge the NATO AVT organization for sponsoring the activity on which this study is a small part, to the UK DSTL and the US Air Force for funding support for the experiments and ARA and NASA for their support with experimental data and computational analysis. In particular the authors thank Dr Joe Coppin, Dr Brett Hiller and Ms Moira Maina for their particular support in this study.

References

[1] Parker N. T. and Pitman R. N., "Aerodynamic studies of control surfaces on a 40° lambda wing configuration (M2362).", DRA/AS/LBA/CR96070/1, March 1996.

[2] Parker N. T. and Ayres J. C., "Mach and Reynolds number effects on a 40° lambda planform half-wing model (M2389), phase 1 tests.", DERA/AS/ASD/CR97076/1, March 1997.

[3] McParlin, S. and Adamczak, D., "Prediction of Transonic Shock-induced Separation for 40degree Lambda Wings", 41st Aerospace Sciences Meeting and Exhibit, AIAA Paper 2003-599, 2003. doi:10.2514/6.2003-599.

[4] Woods, M. I. & Wood, H. J. "Aerodynamic Characteristics of Lamba Wings", The Aeronautical Journal, April 2000. Pp165-174.

[5] McParlin SC, Bruce RJ, Hepworth AG, Rae AJ. Low speed wind tunnel tests on the 1303 UCAV concept. 24th AIAA Applied Aerodynamics Conference. 2006. https://doi.org/10.2514/6.2006-2985.

[6] S. J. Woolvin. "UCAV Configuration & Performance Trade-Offs". 44th AIAA Aerospace Sciences Meeting and Exhibit. AIAA 2006-1264. Defence Science & Technology Laboratory, Farnborough, GU14 0LX, UK. 2006.

[7] S. Woolvin. "A Conceptual Design Study of the 1303 UCAV Configuration". 24th AIAA applied aerodynamic conference, San Francisco, CA. AIAA 2006-2991. Defence Science & Technology Laboratory, Farnborough, GU14 0LX, UK. 2006.

[8] Atkinson M, Ferguson F. A Computational Fluid Dynamics Investigation of the 1303 UCAV Configuration with Deployable Rao Vortex Flaps. 44th AIAA Aerospace Sciences Meeting and Exhibit. 2006. https://doi.org/10.2514/6.2006-1262

[9] Khalid M, Yuan W, Zhang F. A CFD Study of UCAV 1303 Baseline Model at Cruise Mach Number. 26th International Congress of the Aeronautical Sciences. ICAS 2008. https://www.icas.org/ICAS_ARCHIVE/ICAS2008/PAPERS/615.PDF

[10] Weng Heng C. Flow visualization studies over a UCAV 1303 model. Calhoun Institutional Archive of the Naval Postgraduate School. 2009. https://calhoun.nps.edu/handle/10945/4757.

[11] Frink NT, Tormalm M, Schmidt S. Unstructured CFD Aerodynamic Analysis of a Generic UCAV Configuration. NATO RTO-MP-AVT-170. 2011. Paper No. 25. https://ntrs.nasa.gov/api/citations/20110016545/downloads/20110016545.pdf
[12] Cummings RM, Schütte A. 'Integrated Computational/Experimental Approach to Unmanned Combat Air Vehicle Stability and Control Estimation'. Journal of Aircraft, Vol. 49, No. 6, November–December 2012. https://doi.org/10.2514/1.C031430
[13] Liersch CM, Huber KC. Conceptual Design and Aerodynamic Analyses of a Generic UCAV Configuration. 32nd AIAA Applied Aerodynamics Conference,16-20 June 2014, Atlanta, GA. https://doi.org/10.2514/6.2014-2001216.
[14] Smith, P. D., "A calculation method for the turbulent boundary layer on an infinite yawed wing in compressible, adiabatic flow", *ARC CP* 1268. 1974.
[15] Prince, S.A., Di Pasquale, D. & Garry, K.P., "Progress towards a Rapid Method for Conceptual Aerodynamic Design for Transonic Cruise" AIAA SciTech 2020 Forum, https://arc.aiaa.org/doi/abs/10.2514/6.2020-1286
[16] Ashill, P. R. & Smith, P. D. "An integral method for calculating the effects on turbulent boundary layer development on sweep and taper", RAE Technical Report, TR83053. June 1983.
[17] NATO AVT-298 "Reynolds Number Scaling Effects on Swept Wing Flows", Final Report (to be published).

CFD modelling and simulation on a lambda wing at subsonic speed

Prince, Simon A.

2025-01-06

Prince SA, Rana ZA, Di Pasquale D, et al., (2025) CFD modelling and simulation on a lambda wing at subsonic speed. AIAA SCITECH 2025 Forum, 6-10 January 2025 Orlando, FL. Paper number AIAA 2025-1842

https://doi.org/10.2514/6.2025-1842